Numerical Investigation of Three-Dimensional Active Control of Boundary-Layer Transition

L. D. Kral* and H. F. Fasel†
University of Arizona, Tucson, Arizona 85721

A numerical model is developed for the investigation of boundary-layer transition control of spatially evolving instability waves. Active control of a periodically forced boundary layer in an incompressible fluid is simulated using surface heating techniques. The Navier-Stokes and energy equations are solved using a fully implicit finite-difference/spectral method. Temperature perturbations are introduced locally along finite heater strips to directly attenuate instability waves in the flow. A feedback control loop is employed in which a downstream sensor is used to monitor wall shear stress fluctuations. Active control of small-amplitude two-dimensional and three-dimensional disturbances is shown. Both wave reinforcement and wave attenuation are demonstrated. Active control of the early stages of the nonlinear fundamental breakdown process is also numerically investigated. The high three-dimensional growth rates that are characteristic of the secondary instability process are significantly reduced using either two-dimensional or three-dimensional control inputs to the heater strips. A receptivity study of the processes by which the localized temperature perturbations generate instability waves in the boundary layer is made. It is shown that the boundary layer is more receptive to narrow heater strips in that they maximize the amplitude level of the disturbances in the boundary layer.

Introduction

CONTROL of the laminar-turbulent transition process is of considerable interest in aerodynamics and hydrodynamics. Delay or prevention of transition significantly reduces the viscous drag, although acceleration of transition may be desired to delay separation, to enhance mixing for combustion and chemical reactions, or to simulate higher Reynolds number flows in an experimental facility.

There are basically two approaches to control the transition process. In the first approach the base flow is influenced to alter the stability characteristics. The critical Reynolds number at which the flow becomes unstable is increased or reduced, depending on the modification to the base flow. This approach is characterized as passive control. The second approach to influence the transition process is active control in which the disturbance flow resulting from the instability of the base flow is directly influenced using wave superposition techniques. The active control approach is discussed here.

Active control has been demonstrated in the experimental work of Wehrmann,[1] Schilz,[2] Milling,[3] Gedney,[4] Strykowski and Sreenivasan,[5] Maestrello,[6] Liepmann et al.[7], and Thomas.[8] Wehrmann[1] and Schilz[2] first excited a Tollmien-Schlichting (T-S) wave using a vibrating ribbon and then used a flexible wall built into the flat plate to reduce the growing T-S wave by forcing the flexible wall to move in phase opposition to the wave. Milling[3] utilized two vibrating wires to introduce and control disturbances at the same frequency with phase and amplitude adjustments introduced to the second wire. In the experimental work of Gedney,[4] a T-S wave was excited by sound and then nearly canceled by vibrating the plate near the leading edge at the same frequency as the sound signal. Strykowski and Sreenivasan[5] vibrated a wire in a slot in the plate to produce a disturbance and a second wire in another slot downstream of the first was used to control the disturbance. Maestrello[6] generated instability waves on an airfoil using surface heating strips in a region of favorable pressure gradient and then used sound as a control input at near-normal incidence to reduce the perturbation. Liepmann et al.[7] used heating strips to excite instability waves in the boundary layer. The thin metal strips were flush mounted on the plate and subjected to various forms of time-dependent temperature loading. A second set of heating strips was located downstream in order to control the deliberately excited T-S waves from the first heating element by inputting appropriate amplitude and phase perturbations to the second heating element. In an application of this study, Liepmann and Nosenchuck[9] used one heater strip and a hot film probe downstream to actively control the naturally occurring T-S waves. The probe measured the wall shear stress fluctuations from which a signal was synthesized to drive the heater strip out of phase with the T-S waves, forming a feedback control loop. Thomas[8] has studied the development of the flowfield in the boundary layer downstream of the active control measures. By using two vibrating ribbons for the generation and control of the instability waves, transition was delayed. However, downstream of the control measures very weak three-dimensional background disturbances in the flow interacted with the primary two-dimensional waves, and the flow could not be completely restored to its undisturbed state. The appearance of three-dimensional structures was significantly delayed when the control measures were applied.

In addition to the experimental studies, several numerical investigations of active control have been undertaken recently. Two-dimensional numerical investigations of active control of the boundary layer and channel have been made by McMurray et al.,[10] Bayliss et al.,[11] and Bower et al.[12] McMurray et al.[10] have used the temporal stability model in which the flow was assumed to be periodic in the streamwise direction. The disturbances then evolved in time. Control was achieved using periodic wall motion. Bayliss et al.[11] have numerically studied active control of the spatially growing compressible boundary layer. Amplitude reductions of 6% for heating and 12% for cooling were achieved. Bower et al.[12] have numerically investigated active control of a single-frequency wave in the plane channel using periodic wall suction and blowing. The computational model was based on the solution of the Orr-Sommerfeld equation and an analytical expression was derived to provide the amplitude and phase of the downstream surface velocity distribution, which resulted in the suppression of the

Presented as Paper 89-0984 at the AIAA 2nd Shear Flow Conference, Tempe, AZ, March 13-16, 1989; received March 23, 1990; revision received July 9, 1990; accepted for publication July 24, 1990.

*Research Scientist; currently at McDonnell Douglas Research Laboratories, P.O. Box 516, St. Louis, MO 63166. Member AIAA.

†Professor, Aerospace and Mechanical Engineering. Member AIAA.

instability wave. This computational technique has been extended to include wave packet disturbances[13,14] and periodic surface heating.[15] Three-dimensional numerical simulations of active control have been conducted by Kleiser and Laurien,[16,17] Biringen et al.,[18] and Zang and Hussaini.[19,20] In all of these simulations the temporal stability model was used. Kleiser and Laurien[16,17] have applied periodic wall suction and blowing, fluctuating mass forces, and direct manipulation of Fourier modes as control inputs. Biringen et al.[18] have applied periodic suction and blowing to control the flow. Zang and Hussaini[19,20] have performed similar three-dimensional temporal simulations of the boundary layer and plane channel in which they directly suppressed spanwise velocity and pressure modes, leading to a delay in transition.

Important contributions have been made in the numerical investigations of active control of boundary-layer transition. However, for simplicity, streamwise periodicity of the flow and/or a parallel mean flow was assumed (with the exception of the two-dimensional spatial simulations of Bayliss et al.[11]). However, nonparallel effects and the proper wave dispersion can be incorporated only in spatial models. This aspect is particularly important for active control so that accurate changes in phase and amplitude can be determined for input to the control device. In addition, the feedback control loop (as in the experiments of Liepmann and Nosenchuck[9]) can be realized only within the spatial framework with feedback control applied in the streamwise direction.

In this numerical investigation three-dimensional transition control for the spatially developing boundary layer is considered. Active control is accomplished using periodic surface heating. The numerical model allows for investigations of spatially growing, three-dimensional disturbance waves in a growing two-dimensional boundary layer and includes nonparallel effects. The numerical method is based on the algorithm developed by Fasel et al.[21]

In order to gain an understanding of the control aspects of transition, small-amplitude disturbances are first considered. Control of both the two-dimensional T-S waves and the three-dimensional oblique waves is discussed. Through the simulation of linear oblique waves, the applicability of the numerical model for investigating three-dimensional transition control can then be verified. A similar surface heating strip arrangement and feedback control loop is employed, as was demonstrated in the control experiments of Liepmann and Nosenchuck.[9] Although these experiments were two-dimensional, the extension to control of three-dimensional, small-amplitude disturbances is considered to be straightforward. Robey[22] and Corke[23] have triggered three-dimensional waves in the boundary layer by subjecting the heating strips to three-dimensional time-dependent temperature loading.

The process by which localized heat disturbances are initially generated into T-S waves in the boundary layer is also investigated. This process is referred to as receptivity as first put forth by Morkovin.[24] In an analytical study of boundary layer receptivity, Heinrich et al.[25] investigated leading-edge receptivity to freestream disturbances and also the receptivity produced by the interaction of acoustic waves with passive suction slots. For the case of suction along a finite strip the maximum receptivity was found to occur for very narrow suction strips of less than one T-S wavelength, and receptivity was minimized for strip length equal to one T-S wavelength. In the analysis the mass flux at the wall was held constant. Wlezien[26] has experimentally validated the slot receptivity mechanism predicted by Heinrich et al.[25] In this work the receptivity of the boundary layer to the short scale variation in wall heating is examined. The motivation for this study is to determine an optimal length of the heater strip in order to maximize the receptivity of the boundary layer. Therefore, more efficient heater strips can be designed that require a minimal heat input.

Finally, active control applied at the early stages of the nonlinear secondary instability process is shown. Active control of fundamental breakdown is simulated with the uncontrolled flow conditions similar to the laboratory experiments of Klebanoff et al.[27] Either a large-amplitude two-dimensional or a small-amplitude three-dimensional control input to the surface heater strip is introduced, and a comparison of the influence on the three-dimensional growth is made.

Governing Equations and Boundary Conditions

The three-dimensional Navier-Stokes equations, in vorticity transport formulation, are coupled with the energy equation through the temperature-dependent viscosity $\mu = \mu(T)$. The fluid considered in this investigation is water, and all other fluid properties are assumed to be constant since the specific heat, density, and thermal conductivity vary little with temperature. The vorticity vector field ω is denoted by $\omega = [\omega_x, \omega_y, \omega_z]$, and the velocity vector field U is denoted by $U = [u, v, w]$ in the x, y, and z directions, respectively. The vorticity transport and energy equations are given by

$$\frac{D\omega}{Dt} - (\omega \cdot \nabla_1)U = \frac{\mu}{Re}\nabla_1^2\omega + c \tag{1}$$

$$\frac{DT}{Dt} = \frac{1}{RePr}\nabla_1^2 T \tag{2}$$

where

$$\nabla_1 = \frac{\partial}{\partial x}i + \frac{\partial}{\partial y}j + \frac{\partial}{\partial z}k$$

$$\nabla_1^2 = \frac{\partial^2}{\partial x^2} + Re\frac{\partial^2}{\partial y^2} + \frac{\partial^2}{\partial z^2}$$

and

$$\begin{aligned} c_x = {} & +\frac{1}{Re}\frac{\partial\mu}{\partial x}\left(\frac{\partial\omega_x}{\partial x}\right) - \frac{\partial\mu}{\partial y}\left(\frac{1}{Re}\frac{\partial\omega_y}{\partial x} - 2\frac{\partial\omega_x}{\partial y}\right) \\ & + \frac{1}{Re}\frac{\partial\mu}{\partial z}\left(2\frac{\partial\omega_x}{\partial z} - \frac{\partial\omega_z}{\partial x}\right) - \frac{1}{Re}\frac{\partial^2\mu}{\partial x\partial y}\left(\frac{\partial u}{\partial z} + \frac{\partial w}{\partial x}\right) \\ & - \frac{2}{Re}\frac{\partial^2\mu}{\partial y\partial z}\left(\frac{\partial w}{\partial z} - \frac{\partial v}{\partial y}\right) + \frac{1}{Re}\frac{\partial^2\mu}{\partial x\partial z}\left(\frac{\partial u}{\partial y} + \frac{1}{Re}\frac{\partial v}{\partial x}\right) \\ & - \left(\frac{\partial^2\mu}{\partial y^2} - \frac{1}{Re}\frac{\partial^2\mu}{\partial z^2}\right)\left(\frac{1}{Re}\frac{\partial v}{\partial z} + \frac{\partial w}{\partial y}\right) \end{aligned}$$

$$\begin{aligned} c_y = {} & +\frac{\partial\mu}{\partial x}\left(\frac{2}{Re}\frac{\partial\omega_y}{\partial x} - \frac{\partial\omega_x}{\partial y}\right) + \frac{\partial\mu}{\partial y}\left(\frac{\partial\omega_y}{\partial y}\right) \\ & - \frac{\partial\mu}{\partial z}\left(\frac{\partial\omega_z}{\partial y} - \frac{2}{Re}\frac{\partial\omega_y}{\partial z}\right) + \frac{\partial^2\mu}{\partial x\partial y}\left(\frac{1}{Re}\frac{\partial v}{\partial z} + \frac{\partial w}{\partial y}\right) \\ & - \frac{\partial^2\mu}{\partial y\partial z}\left(\frac{\partial u}{\partial y} + \frac{1}{Re}\frac{\partial v}{\partial x}\right) - \frac{2}{Re}\frac{\partial^2\mu}{\partial x\partial z}\left(\frac{\partial u}{\partial x} - \frac{\partial w}{\partial z}\right) \\ & - \left(\frac{1}{Re}\frac{\partial^2\mu}{\partial z^2} - \frac{\partial^2\mu}{\partial x^2}\right)\left(\frac{\partial u}{\partial z} + \frac{\partial w}{\partial x}\right) \end{aligned}$$

$$\begin{aligned} c_z = {} & -\frac{1}{Re}\frac{\partial\mu}{\partial x}\left(\frac{\partial\omega_x}{\partial z} - \frac{\partial\omega_z}{\partial x}\right) + \frac{\partial\mu}{\partial y}\left(2\frac{\partial\omega_z}{\partial y} - \frac{1}{Re}\frac{\partial\omega_y}{\partial z}\right) \\ & + \frac{1}{Re}\frac{\partial\mu}{\partial z}\left(\frac{\partial\omega_z}{\partial z}\right) - \frac{2}{Re}\frac{\partial^2\mu}{\partial x\partial y}\left(\frac{\partial v}{\partial y} - \frac{\partial u}{\partial x}\right) \\ & + \frac{1}{Re}\frac{\partial^2\mu}{\partial y\partial z}\left(\frac{\partial u}{\partial z} - \frac{\partial w}{\partial x}\right) - \frac{1}{Re}\frac{\partial^2\mu}{\partial x\partial z}\left(\frac{1}{Re}\frac{\partial v}{\partial z} + \frac{\partial w}{\partial y}\right) \\ & - \left(\frac{1}{Re}\frac{\partial^2\mu}{\partial x^2} - \frac{\partial^2\mu}{\partial y^2}\right)\left(\frac{\partial u}{\partial y} + \frac{1}{Re}\frac{\partial v}{\partial x}\right) \end{aligned}$$

The Reynolds number is defined by $Re = \rho U_\infty L/\mu_\infty$, where U_∞ is the freestream velocity, L is a reference length, μ_∞ is the freestream dynamic viscosity, and ρ is the density. The Prandtl number is defined by $Pr = \mu_\infty c/k$, where c is the specific heat and k is the thermal conductivity. All variables in Eqs. (1) and (2) are nondimensionalized as follows:

$$x = \frac{\bar{x}}{L}, \qquad y = \frac{\bar{y}}{L}\sqrt{Re}, \qquad z = \frac{\bar{z}}{L}$$

$$u = \frac{\bar{u}}{U_\infty}, \qquad v = \frac{\bar{v}}{U_\infty}\sqrt{Re}, \qquad w = \frac{\bar{w}}{U_\infty} \tag{3}$$

$$t = \frac{\bar{t}U_\infty}{L}, \qquad T = \frac{\bar{T}-T_\infty}{T_w-T_\infty} \qquad \mu = \frac{\bar{\mu}}{\mu_\infty}$$

where the subscript w represents the wall value, and the subscript ∞ represents freestream conditions. Note that a $\sqrt{Re}$ scaling is made in the normal direction. The nondimensional vorticity components are given by

$$\omega_x = \frac{1}{Re}\frac{\partial v}{\partial z} - \frac{\partial w}{\partial y} \tag{4a}$$

$$\omega_y = \frac{\partial w}{\partial x} - \frac{\partial u}{\partial z} \tag{4b}$$

$$\omega_z = \frac{\partial u}{\partial y} - \frac{1}{Re}\frac{\partial v}{\partial x} \tag{4c}$$

From the definition of vorticity and the continuity equation,

$$\nabla_1 \cdot U = 0 \tag{5}$$

three Poisson equations are derived for the three velocity components:

$$\nabla_2^2 u = -\frac{\partial \omega_y}{\partial z} - \frac{\partial^2 v}{\partial x \partial y} \tag{6a}$$

$$\frac{1}{Re}\nabla_1^2 v = \frac{\partial \omega_x}{\partial z} - \frac{\partial \omega_z}{\partial x} \tag{6b}$$

$$\nabla_2^2 w \frac{\partial \omega_y}{\partial x} - \frac{\partial^2 v}{\partial y \partial z} \tag{6c}$$

where

$$\nabla_2^2 = \frac{\partial^2}{\partial x^2} + \frac{\partial^2}{\partial z^2}$$

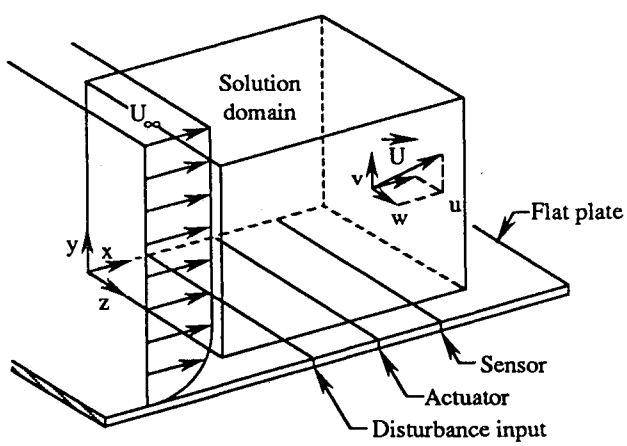

Fig. 1 Schematic illustration of spatial domain and coordinate system for numerical simulations of active control.

The numerical method is based on the solution of Eqs. (1), (2), and (6) for the three vorticity components, the temperature, and the three velocity components. To complete the equation system, an empirical relationship between the viscosity and temperature is used.[28,29]

The base flow is two-dimensional and is represented by the velocity components $U = [u_B, v_B]$, the vorticity ω_{zB}, and the temperature T_B. The base flow is obtained by solving Eqs. (1), (2), and (6) for steady, two-dimensional, incompressible flow with $\partial/\partial z = 0$, $w = 0$, $\omega_x = 0$, and $\omega_y = 0$.

Integration Domain

The coordinate system and spatial domain are shown in Fig. 1. The governing equations are solved in the x direction from $x = x_0$ to $x = x_N$, where x_0 is downstream of the leading edge. The integration domain in the y direction extends from $y = 0$ to $y = y_M$ and covers several boundary-layer thicknesses. The flow is assumed periodic in the spanwise direction with the domain extending from $z = 0$ to $z = \lambda_z$, where λ_z is the spanwise wavelength.

Boundary Conditions

The boundary conditions employed for the base flow are as follows. At the inflow boundary, $x = x_0$, the Blasius similarity solution is imposed:

$$u_B(x_0,y) = u_{\text{Blas}}(x_0,y) \tag{7a}$$

$$v_B(x_0,y) = v_{\text{Blas}}(x_0,y) \tag{7b}$$

$$\omega_{zB}(x_0,y) = \omega_{z\text{Blas}}(x_0,y) \tag{7c}$$

$$T_B(x_0,y) = 0 \tag{7d}$$

At the ouflow boundary, $x = x_N$, the following conditions are employed:

$$\frac{\partial u_B}{\partial x}(x_N,y) = -\frac{\partial v_B}{\partial y}(x_N,y) \tag{8a}$$

$$\frac{\partial^2 v_B}{\partial x^2}(x_N,y) = 0 \tag{8b}$$

$$\frac{\partial^2 \omega_{zB}}{\partial x^2}(x_N,y) = 0 \tag{8c}$$

$$\frac{\partial^2 T_B}{\partial x^2}(x_N,y) = 0 \tag{8d}$$

Equations (8) are derived from a consideration of the boundary-layer equations and the continuity equation. At the outer boundary, $y = y_M$, the following conditions are enforced:

$$u_B(x,y_M) = 1 \tag{9a}$$

$$\frac{\partial v_B}{\partial y}(x,y_M) = 0 \tag{9b}$$

$$\omega_{zB}(x,y_M) = 0 \tag{9c}$$

$$T_B(x,y_M) = 0 \tag{9d}$$

Equation (9a) shows that no freestream pressure gradient is imposed. The freestream boundary is positioned far away from the wall so that Eqs. (9c) and (9d) are justified. At the wall, $y = 0$, the following conditions are imposed:

$$u_B(x,0) = 0 \tag{10a}$$

$$v_B(x,0) = 0 \tag{10b}$$

$$\frac{\partial v_B}{\partial y}(x,0) = 0 \tag{10c}$$

$$\frac{\partial \omega_{zB}}{\partial x}(x,0) = \frac{\partial^2 v_B}{\partial y^2}(x,0) \tag{10d}$$

$$T_B(x,0) = \begin{cases} T_{Bw}(x) & \text{if } x_{HB_i} \le x \le x_{HE_i} \\ 0 & \text{otherwise} \end{cases} \tag{10e}$$

where $i = 1$, NHS, and NHS denotes the number of heater strips activated. Each heater strip is employed from $x_{HB_i} \le x \le x_{HE_i}$. This local temperature distribution at the wall represents a steady-state overheat due to the presence of the heater strip.

For the calculation of the unsteady three-dimensional disturbance flow, the following boundary conditions for the disturbances are used. At the inflow boundary, all disturbances are assumed to be zero, or

$$\psi(x_0,y,z,t) = 0 \tag{11}$$

where $\psi = \{u,v,w,\omega_x,\omega_y,\omega_z,T\}$. At the outflow plane, a moving boundary is employed that is propagated sufficiently ahead of the disturbance wave. This moving boundary prevents wave reflections and reduces computational time. At this moving boundary, the following boundary condition is employed:

$$\frac{\partial^2 \psi}{\partial x^2}(x_N,y,z,t) = -\alpha_{r_N}^2 \psi(x_N,y,z,t) \tag{12}$$

This condition assumes that the disturbances are periodic in x with a local wave number α_{r_N}. This radiation condition is sufficient for small growth rates, but the moving boundary is found to be necessary for larger growth rates. At the outer boundary, exponential decay for the v perturbation velocity is assumed:

$$\frac{\partial v}{\partial y}(x,y_M,z,t) = -\frac{\alpha^*}{\sqrt{Re}} v(x,y_M,z,t) \tag{13a}$$

where α^* is a wave number. The choice of α^* is discussed in conjunction with the numerical method. Again, the freestream boundary is positioned far enough from the wall so that the vorticity and temperature perturbations are assummed to be zero there:

$$\omega(x,y_M,z,t) = 0 \tag{13b}$$

$$T(x,y_M,z,t) = 0 \tag{13c}$$

At the wall, no-slip conditions are employed:

$$u(x,0,z,t) = 0 \tag{14a}$$

$$w(x,0,z,t) = 0 \tag{14b}$$

The v perturbation velocity component at the wall is a prescribed function of x, z, and t:

$$v(x,0,z,t) = \begin{cases} v_w(x,z,t) & \text{if } x_{SB_1} \le x \le x_{SE_1} \\ 0 & \text{otherwise} \end{cases} \tag{14c}$$

This condition allows for localized time-dependent disturbances to be introduced into the flowfield and is used to simulate a suction and blowing strip. For the three vorticity components at the wall, the following boundary conditions are used:

$$\frac{\partial^2 \omega_x}{\partial x^2}(x,0,z,t) + \frac{\partial^2 \omega_x}{\partial z^2}(x,0,z,t) = -\frac{\partial^2 \omega_y}{\partial x \partial y}(x,0,z,t) + \frac{1}{Re}\frac{\partial}{\partial z}[\nabla_1^2 v(x,0,z,t)] \tag{14d}$$

$$\omega_y(x,0,z,t) = 0 \tag{14e}$$

$$\frac{\partial \omega_z}{\partial x}(x,0,z,t) = \frac{\partial \omega_x}{\partial z}(x,0,z,t) - \frac{1}{Re}\nabla_1^2 v(x,0,z,t) \tag{14f}$$

These equations result from the definition of vorticity and the continuity equation. The wall boundary condition for the temperature perturbation is similar to the v velocity component:

$$T(x,0,z,t) = \begin{cases} T_w(x,z,t) & \text{if } x_{HB_i} \le x \le x_{HE_i} \\ 0 & \text{otherwise} \end{cases} \tag{14g}$$

This boundary condition allows for time-periodic localized wall heating. Finally, for the spanwise boundaries at $z = 0$ and $z = \lambda_z$, periodicity conditions are employed. Thus, for all variables,

$$\psi(x,y,0,t) = \psi(x,y,\lambda_z,t) \tag{15}$$

Numerical Method

The numerical method is a combined finite-difference/spectral technique in which finite differences are employed in the x and y directions and a spectral representation is used in the z direction. Since the flow is assumed to exhibit spanwise periodicity, a finite Fourier series is used:

$$\psi(z) \simeq \sum_{k=-K/2}^{k=K/2} \Psi_k e^{ik\gamma z} \tag{16}$$

where $\Psi = (U,V,W,\Omega_x,\Omega_y,\Omega_z,\Theta)$, and γ is the spanwise wave number (related to the spanwise wavelength by $\gamma = 2\pi/\lambda_z$).

The following nonlinear terms are first defined in physical space:

$$\boldsymbol{a} = (\boldsymbol{U}\cdot\nabla_1)\boldsymbol{\omega} - (\boldsymbol{\omega}\cdot\nabla_1)\boldsymbol{U} \tag{17a}$$

$$\boldsymbol{b} = \frac{\mu}{Re}\nabla_1^2\boldsymbol{\omega} \tag{17b}$$

$$d = (\boldsymbol{U}\cdot\nabla_1)T \tag{17c}$$

where $\boldsymbol{a}$ is the vector $\boldsymbol{a} = [a_x,a_y,a_z]$, $\boldsymbol{b}$ is the vector $\boldsymbol{b} = [b_x,b_y,b_z]$, and the vector $\boldsymbol{c}$ is already defined. The nonlinear term for the energy equation, d, is a scalar. Note that since viscosity varies with temperature, $\boldsymbol{b}$ is also a nonlinear term.

Substitution of the preceding relations into Eqs. (1), (2), and (6) yields a new set of governing equations in terms of Fourier modes rather than physical variables. The resulting equation system is

$$\frac{\partial \Omega_{x_k}}{\partial t} + A_{x_k} = B_{x_k} + C_{x_k} \tag{18a}$$

$$\frac{\partial \Omega_{y_k}}{\partial t} + A_{y_k} = B_{y_k} + C_{y_k} \tag{18b}$$

$$\frac{\partial \Omega_{z_k}}{\partial t} + A_{z_k} = B_{z_k} + C_{z_k} \tag{18c}$$

$$\frac{\partial^2 U_k}{\partial x^2} - \gamma^2 k^2 U_k = -i\gamma k \Omega_{y_k} - \frac{\partial^2 V_k}{\partial x \partial y} \tag{18d}$$

$$\frac{1}{Re}\frac{\partial^2 V_k}{\partial x^2} + \frac{\partial^2 V_k}{\partial y^2} - \frac{\gamma^2 k^2}{Re} V_k = i\gamma k \Omega_{x_k} - \frac{\partial \Omega_{z_k}}{\partial x} \tag{18e}$$

$$\frac{\partial^2 W_k}{\partial x^2} - \gamma^2 k^2 W_k = \frac{\partial \Omega_{y_k}}{\partial x} - i\gamma k \frac{\partial V_k}{\partial y} \tag{18f}$$

$$\frac{\partial \Theta_k}{\partial t} + D_k = \frac{1}{Re\,Pr}\frac{\partial^2 \Theta_k}{\partial x^2} + \frac{1}{Pr}\frac{\partial^2 \Theta_k}{\partial y^2} - \frac{\gamma^2 k^2}{Re\,Pr}\Theta_k \tag{18g}$$

for

$$k = (-K/2, \ldots, -1, 0, 1, \ldots, K/2)$$

With this spectral approximation the following choice of α^* in the boundary condition for the freestream velocity has been shown to be[21]

$$\alpha_k^* = \sqrt{\alpha^2 + \gamma^2 k^2}$$

Equations (18) are discretized using finite-difference approximations of second-order accuracy in the x and y directions. The time derivatives are approximated by second-order backward differences. The numerical method is a fully implicit line iteration procedure. A detailed description of the numerical procedure is given by Kral.[30]

Generation and Control of Disturbances

The discrete set of equations is solved first for the two-dimensional base flow. The disturbances are then introduced into the solution domain for $t > 0$. The disturbances are introduced either through a suction and blowing strip or a surface heater strip. The choice of disturbance input is discussed in the next section. Figure 1 shows the localized strip locations. A surface heater strip is located downstream of the disturbance input and serves as the actuator. The wall sensor location is also shown. For a disturbance introduced with periodic suction and blowing and controlled with periodic surface heating, wall boundary conditions (14c) and (14g) employed over the strips become in Fourier space

$$V_{w_k}(x,z,t) = \epsilon_{V_k} \hat{V}_{w_k}(x)\, \sin(\beta_k t) \tag{19a}$$

$$\Theta_{w_k}(x,z,t) = H(t-t_1)\, \epsilon_{\Theta_k} \hat{\Theta}_{w_k}(x)\, \sin(\beta_k t + \Delta\phi_k) \tag{19b}$$

where ϵ_{V_k} and ϵ_{Θ_k} are amplitude inputs, β_k is the dimensionless frequency, $H(t-t_1)$ is the Heaviside function, and t_1 denotes the time at which the actuator heater strip is initiated. The phase is adjusted by the parameter $\Delta\phi_k = j\pi - \Delta\phi_k^*$, where $j = 1$ for attenuation and $j = 2$ for reinforcement. The x distribution is prescribed through $\hat{V}_{w_k}(x)$ and $\hat{\Theta}_{w_k}(x)$, respectively. For a disturbance introduced with periodic surface heating and also controlled with periodic heating, the following wall boundary conditions are imposed:

$$V_{w_k}(x,z,t) = 0 \tag{20a}$$

over the first heater strip:

$$\Theta_{w_k}(x,z,t) = \epsilon_{\Theta_k} \hat{\Theta}_{w_k}(x)\, \sin(\beta_k t) \tag{20b}$$

and over the second heater strip:

$$\Theta_{w_k}(x,z,t) = H(t-t_1)\, \epsilon_{\Theta_k} \hat{\Theta}_{w_k}(x)\, \sin(\beta_k t + \Delta\phi_k) \tag{20c}$$

The suction and blowing strip and heater strip are spanwise periodic. The two-dimensional disturbance is introduced for $k = 0$, and three-dimensional oblique disturbances are introduced into the solution domain for $k > 0$. The initial disturbance input begins about one disturbance wavelength from the left boundary. The suction and blowing strip covers one T-S wavelength, and the heater strip is one-half of a T-S wavelength in length.

Results

Active control is first applied to small-amplitude, two-dimensional and three-dimensional disturbance waves. This test case provides a check on the numerical method. In particular, the feedback control loop can be verified. Results of a receptivity analysis of a two-dimensional surface heater strip for the small-amplitude test case are also discussed. Finally, results of active control applied to the early stages of the fundamental breakdown process are shown. The Reynolds number and Prandtl number used in these numerical simulations are $Re = 1 \times 10^5$ and $Pr = 6.3$.

Control of Small-Amplitude Disturbances

For the small-amplitude case the following parameters are chosen. The integration domain begins at $Re_{\delta_1}(x_0) = 500$, where Re_{δ_1} is the Reynolds number based on displacement thickness. The integration domain extends for about 16 disturbance wavelengths in the x direction, where approximately 30 grid points are employed per disturbance wavelength. The y domain spans 10 boundary-layer displacement thicknesses at the inflow boundary, and the grid contains 50 intervals in this direction. This time increment is chosen so that there are 60 time steps per period. The disturbances are generated at a frequency of $\beta_0 = \beta_1 = 10$, and the spanwise wave number is $\gamma = 20$. Two Fourier modes are calculated ($K = 2$). For the calculation of active control of small-amplitude disturbances, the disturbance is introduced into the flow using periodic surface heating and is also controlled with a surface heater strip [Eqs. (20)]. The disturbance amplitudes $\epsilon_{\Theta_0}$and ϵ_{Θ_1} are chosen so that the temperature perturbations create small-amplitude disturbance velocities of approximately 0.05% of the maximum freestream velocity. They are also chosen so that the temperature input from the heater strip represents heating only and no cooling. This representation for the heater strip is implemented by the addition of the steady-state component [Eq. (10e)] to the oscillating component. This heater strip design follows the experimental work of Liepmann and Nosenchuck,[9] in which both dc (mean temperature) and ac (sinusoidal) heating were introduced. The temperature perturbation amplitudes are set at $\epsilon_{\Theta_0} = 2/3$ and $\epsilon_{\Theta_1} = 2/3$. This amplitude input represents a temperature of 2°C above the freestream temperature of 24°C for the oscillatory component with the temperature nondimensionalized by $T_w - T_\infty = 3$°C. The steady-state component over the heater strip has a 3°C increase above the freestream temperature. The functional relationship used over the heater strip is a $\sin^2(x)$ distribution.

The disturbance flow is decomposed into a two-dimensional wave ($k = 0$) and a three-dimensional oblique wave ($k = 1$). The Fourier modes resulting from the time-periodic disturbance input over the heater strip without control applied are shown in Fig. 2 for the U_0 and U_1 streamwise velocities. Perspective representations of each Fourier mode are shown after nine periods have been computed (time step $L = 540$). The two-dimensional mode is shown in Fig. 2a, and the three-dimensional mode is shown in Fig. 2b. The perturbation inputs are introduced just upstream of the lower branch of the neutral curve of both the two-dimensional and three-dimensional disturbances. The decay and then subsequent growth as the neutral curve is crossed can be observed. The solution domain does not encompass the upper branch of the neutral curve.

The downstream sensor monitors the spanwise wall vorticity (hence the wall shear stress). An appropriate phase relationship is then found between the sensor and actuator for controlling the instability waves. Several observations are made concerning the signal to the actuator. First, the amplitude input to the second heater strip is the same as that input to the initial heater strip. Therefore, the amplification or damping that takes place between the two surface heater strips is not compensated for in these simulations. However, since the two heater strips are near the neutral curve, the amplification rates are small. Second, the phase is adjusted by the parameter

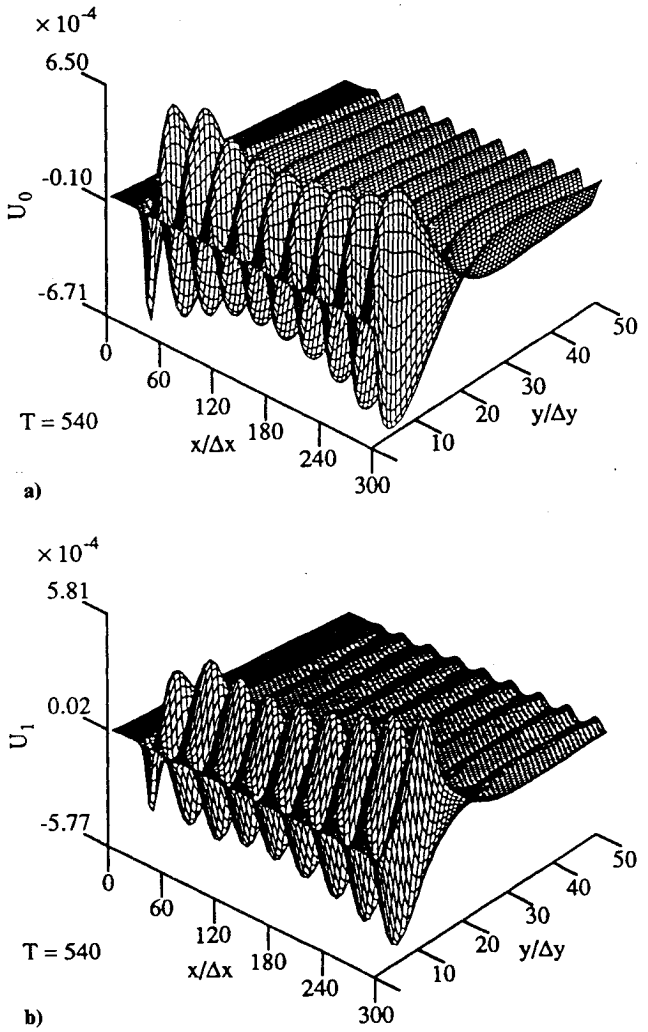

Fig. 2 Fourier modes of the uncontrolled disturbed flow with the disturbance introduced using a surface heater strip located between 30 $\leq x/\Delta x \leq 45$; a) for two-dimensional streamwise velocity U_0; and b) for three-dimensional streamwise velocity U_1.

$\Delta\phi_k = j\pi - \Delta\phi_k^*$. The phase adjustments $\Delta\phi_k^*$ are determined at the downstream sensor. The phase change is calculated by

$$\Delta\phi_k^* = \alpha_{r_k}\Delta x \tag{21}$$

where α_{r_k} is the wave number based on the spanwise wall vorticity Ω_{z_k}. The length Δx is the distance between the sensor and the actuator. For these active control simulations the sensor is located at $x/\Delta x = 240$ ($Re_{\delta_1} = 885$), or about four T-S wavelengths downstream of the actuator. The phase inputs are calculated from the spanwise vorticity disturbances with just the first heater strip activated. These phase inputs are summarized in Table 1.

Two numerical simulations of active control of small-amplitude disturbances are run. The first case is with $j = 1$ so that the actuator introduces disturbances that are out of phase with the disturbances in the flow. The second case is with $j = 2$ so that the temperature perturbations introduced at the actuator are in phase with the disturbances in the flowfield. Results of both cases are now discussed.

The Fourier modes for the U_0 and U_1 velocities that result from the application of the second heater strip are shown in Figs. 3 and 4. Figure 3 shows the results for the out-of-phase control (or $j = 1$), and Fig. 4 shows the velocity perturbations with the in-phase control (or $j = 2$) applied. Both the two-dimensional and three-dimensional modes show a strong reduction downstream of the actuator for the out-of-phase input, whereas a strong increase in amplitude can be seen for the in-phase case.

Table 1 Parameters for active control of small amplitude disturbances

k	α_{r_k}	$\Delta\phi_k^*$,rad
0	28.094	0.096
1	26.694	4.871

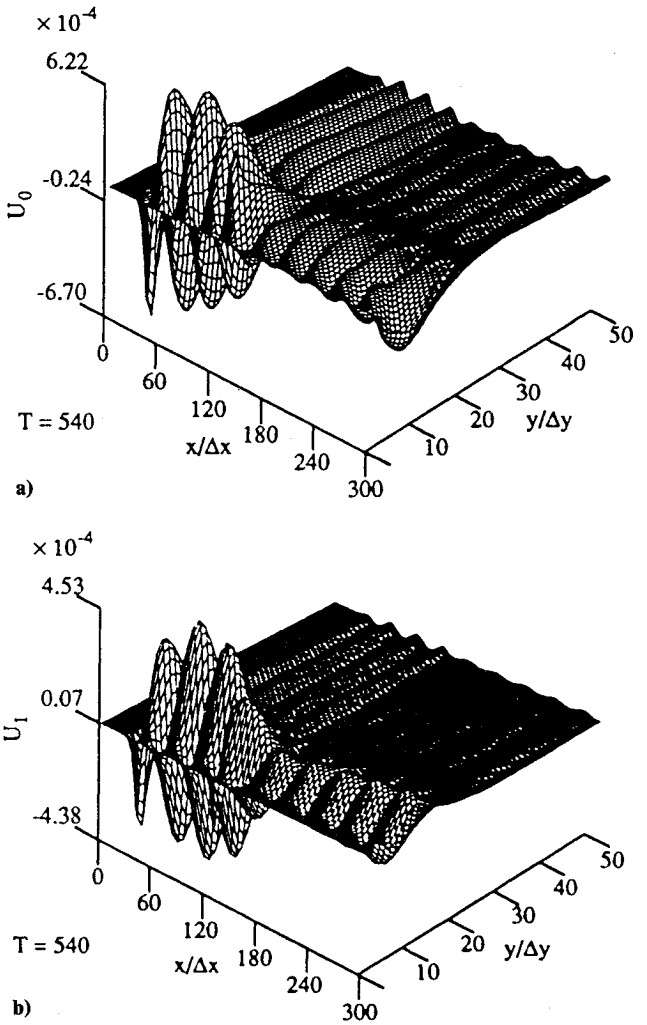

Fig. 3 Fourier modes of the disturbed flow with out-of-phase active control applied using an actuator located between $120 \leq x/\Delta x \leq 135$ and sensor at $x/\Delta x = 240$; a) for two-dimensional streamwise velocity U_0; and b) for three-dimensional streamwise velocity U_1.

A comparison of the active control simulations with the uncontrolled flow is shown in Fig. 5, in which the amplitude profiles for the U_0 and U_1 velocities are plotted. The profiles are shown at the downstream sensor location of $x/\Delta x = 240$. The amplitude levels are strongly reduced for the out-of-phase perturbations and significantly increased with in-phase temperature perturbations applied. It is noted that total cancellation is not achieved for the in-phase heater strip case. If an adjustment in the amplitude levels had been made, an even larger reduction would probably have resulted. However, the reduction in amplitude levels is already quite significant.

Figure 6 shows the amplitude growth downstream for the U_0 and U_1 velocities for both active control cases, as well as for the uncontrolled case. The strong reduction (or increase) in the amplitudes occurs shortly downstream of the actuator input, but the growth rates are not altered since the base flow is not influenced, except locally over the heater strip.

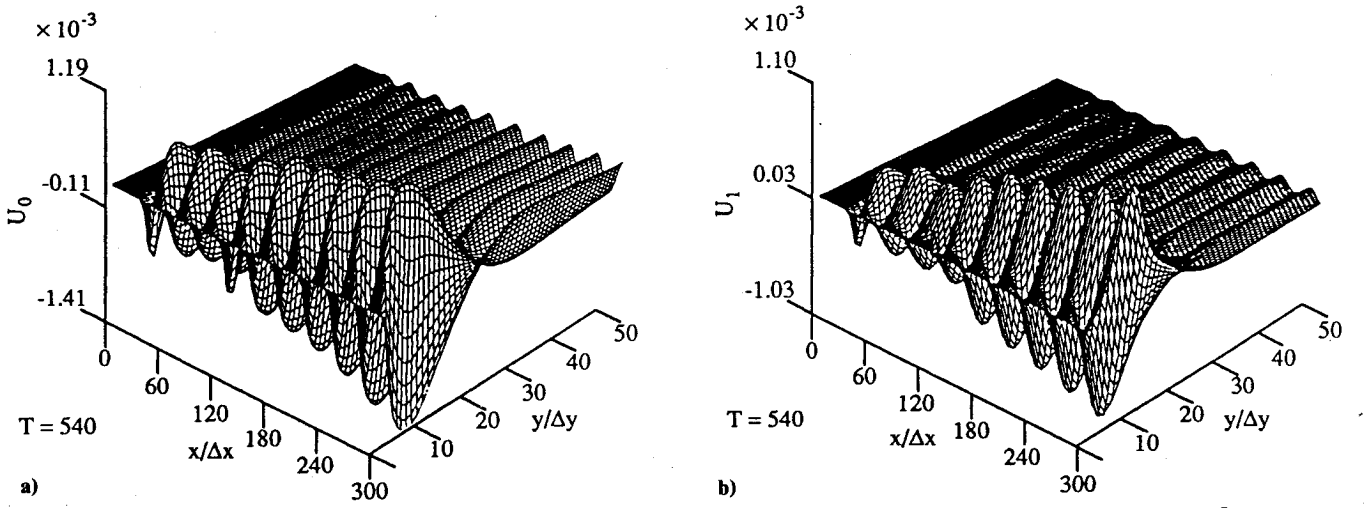

Fig. 4 Fourier modes of the disturbed flow with in-phase active control applied using an actuator located between $120 \le x/\Delta x \le 135$ and sensor at $x/\Delta x = 240$; a) for two-dimensional streamwise velocity U_0 and b) for three-dimensional streamwise velocity U_1.

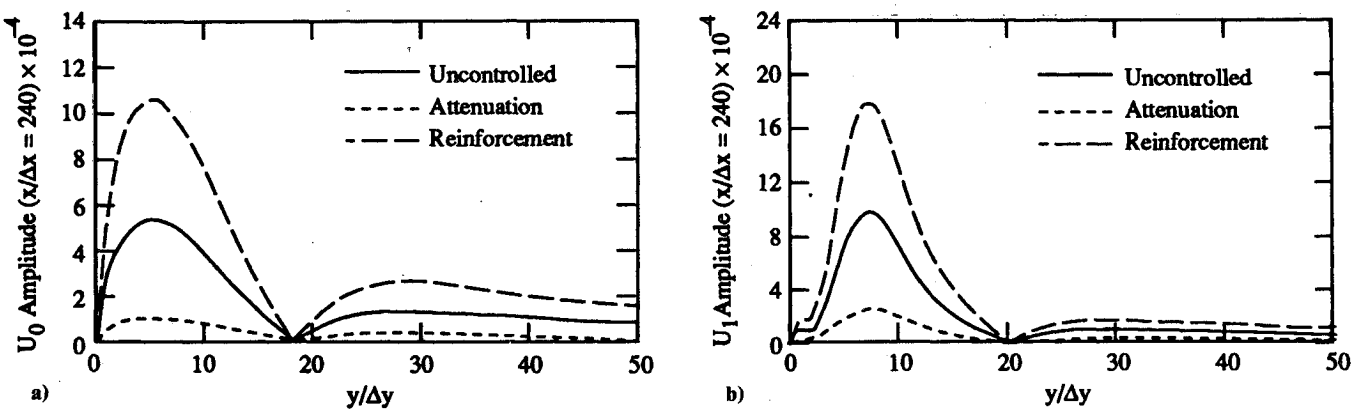

Fig. 5 Comparison of amplitude profiles with active control applied; a) for two-dimensional streamwise velocity U_0 and b) for three-dimensional streamwise velocity U_1.

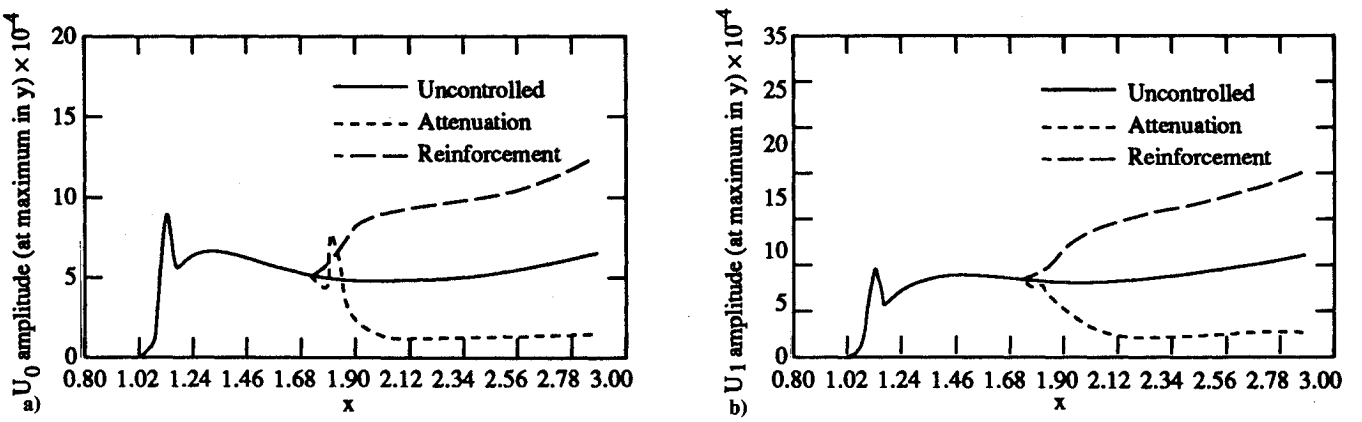

Fig. 6 Influence of active control on the streamwise amplitude growth: a) for two-dimensional streamwise velocity U_0; and b) for three-dimensional streamwise velocity U_1.

Receptivity of a Surface Heater Strip

The receptivity of the boundary layer to the localized temperature perturbations is examined. By understanding the receptivity mechanisms of a discrete surface heater, more efficient heater strips can be designed to maximize (or minimize, depending on the application) a disturbance input. In addition, by understanding the processes by which a localized temperature perturbation creates disturbance waves in the flow, active control can be improved upon.

First, consideration is given to the length (in the streamwise direction) of the heater strip. The streamwise temperature distribution for the heater strip is of the form $\sin^2(x)$. This shape function was chosen to approximately simulate a physical heater strip. Although the shape function also plays a role in the receptivity mechanisms (as shown in the work of Heinrich et al.[25]), only the variation in the heater strip length is considered in this receptivity analysis. Four discrete lengths are studied in fractions of a two-dimensional T-S wavelength (i.e., $d_{HS}/\lambda_{TS} = 1/4$, 1/2, 3/4, and 1), where d_{HS} is the length of the heater strip, and λ_{TS} is the T-S wavelength. Only a receptivity analysis of the two-dimensional heater strip is considered, but a similar numerical analysis could be considered

for three-dimensional oblique waves. An analytical receptivity analysis of three-dimensional wall suction and roughness has been made by Choudari and Kerschen.[31] For this application the maximum receptivity is desired, or the maximum disturbance amplitude created for the smallest heat input to the heater strip. A constant amount of heat transfer, as an input parameter, is not easily maintainable in the numerical simulation. Therefore, the parameter ϵ_{θ_0}, representing a temperature difference ΔT, is varied. Four different temperature disturbance amplitudes are considered: $\epsilon_{\theta_0} = 1/3$, 1.5/3, 2/3, and 2.5/3. Thus, for each ratio of d_{HS}/λ_{TS} four different levels of heating are considered. Figure 7 shows a comparison between the heat transferred over the heater strip and the level of heating (or ΔT) for the four different ratios of d_{HS}/λ_{TS}. The heat transferred increases with each incremental increase in heating. The wider heater strips also have larger heat inputs due to the larger surface area. To determine the most efficient length of heater strip, the amplitude of the two-dimensional wall vorticity is monitored at a downstream location of about seven T-S wavelengths. The amplitude level created by the time-dependent temperature perturbation input vs the amount of heat input for each disturbance wavelength is shown in Fig. 8. It is observed from this figure that the smaller heater strips are able to produce larger disturbances for an equivalent heat input. Thus, the boundary layer is more receptive to the narrower heater strips in terms of maximizing the disturbance levels in the flowfield.

Although Heinrich et al.[25] considered the interaction of an acoustic wave and a discrete suction slot, the results of their analysis are in qualitative agreement with the results of this numerical investigation for a discrete heater strip. They found the boundary layer more receptive to narrow suction strips.

In the experimental work of Nosenchuck[32] and the analytic work of Maestrello,[33] an optimal ratio of the length of the heater strip to the displacement thickness was found. Nosenchuck found an experimental criterion of

$$2 \leq d_{HS}/\delta_1 \leq 10$$

and Maestrello found an analytical criterion of

$$6 \leq d_{HS}/\delta_1 \leq 10$$

For the different lengths of heater strips examined here, Table 2 shows the ratio of length to displacement thickness. Thus, the 1/4 wavelength heater strip, which provides the highest receptivity, also falls within the criterions of both Nosenchuck and Maestrello.

Although the heater strip of length $d_{HS}/\lambda_{TS} = 1/4$ has the highest slope (or highest ratio of amplitude to heat input), a large temperature difference ϵ_{θ_0} is required to achieve the same amplitude levels as the wider heater strips. A disturbance amplitude of approximately 0.05% of the freestream velocity is desired in the numerical simulations, and the heater strip of length $d_{HS} = 1/2\lambda_{TS}$ and $\epsilon_{\theta_0} = 2/3$ creates waves of this amplitude level. Therefore, this heater strip is chosen for the simulations of active control of small-amplitude disturbances.

Control of Secondary Instability

Results of active control applied at the early stages of the nonlinear three-dimensional secondary instability process are now shown. Control of the fundamental breakdown process is investigated. The parameters chosen for the simulation of secondary instability model as closely as possible the experiments of Klebanoff et al.[27]

The parameters used in the study of active control of the ordered peak-valley breakdown process are as follows. The step size in the streamwise direction x is chosen so that there are approximately 60 grid points per disturbance wavelength. The normal step size is determined so that the y direction spans 6.5 boundary-layer displacement thicknesses at the inflow boundary. The grid has 61 points in the normal direction and 901 points in the streamwise direction. Thus, the streamwise domain contains about 15 disturbance wavelengths. The time discretization is chosen so that there are 100 time steps per disturbance period, and the frequencies for both the two-dimensional and three-dimensional disturbances are $\beta_k = 5.88$. The spanwise wave number is $\gamma = 24.3$. In the region analyzed numerical tests show that two Fourier modes are sufficient to resolve the spanwise flow.

For the active control simulations of secondary instability, the disturbances are introduced through a discrete suction and blowing strip at the wall. The strip is located one disturbance wavelength downstream of the left boundary ($x_{SB_1} = 60$ and $x_{SE_1} = 120$) and covers about one wavelength. The disturbance amplitudes ϵ_{V_0} and ϵ_{V_1} are chosen so that the velocity perturbations create disturbance waves of the same amplitude as that observed in the experiments ($\epsilon_{V_0} = 1.45 \times 10^{-3}$ and $\epsilon_{V_1} = 6.0 \times 10^{-6}$). A fifth-order polynomial is used for the function $\hat{V}_{w_k}(x)$ in Eq. (19a). A suction and blowing strip is employed to introduce the disturbances in the flow, and a surface heater strip is located one-half wavelength downstream to serve as the actuator. The functional relationship over the heater strip is $\sin(x)$. Some difficulties were encountered in attempting active control of secondary instability. For active control to be effective, the amplitude levels that are created at the heater strip must be much larger than those for the small-amplitude control simulations. These higher amplitude levels are difficult to create with a single heater strip and with reasonable temperature inputs; hence, the $\sin(x)$ distribution is used to allow for more heat input than the $\sin^2(x)$ distribution.

Two active control cases are considered. In the first case control of only the two-dimensional wave is attempted. In the second case active control of only the three-dimensional wave component is considered. A comparison is then made of the effectiveness of a two-dimensional control input vs a three-

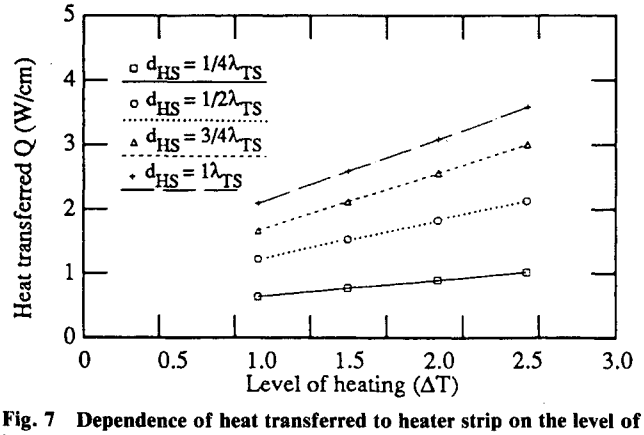

Fig. 7 Dependence of heat transferred to heater strip on the level of heating (ΔT) for four different lengths (d_{HS}) of heater strips.

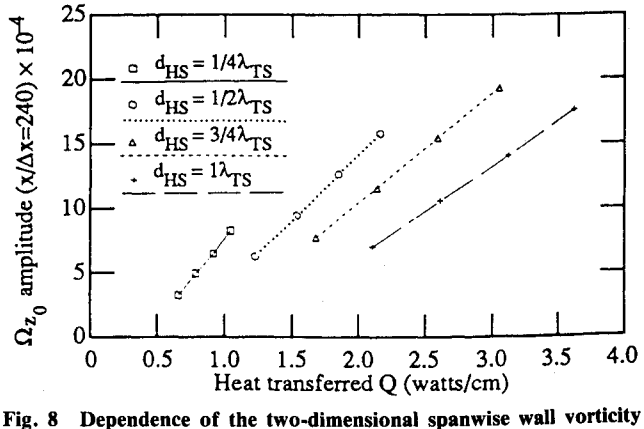

Fig. 8 Dependence of the two-dimensional spanwise wall vorticity amplitude Ω_{z_0} on the amount of heat input and the heater strip length.

Table 2 Comparison of displacement thickness to heater strip length

d_{HS}/λ_{TS}	d_{HS}/δ_1
1/4	9.8
1/2	19.4
3/4	28.8
1	38.0

Table 3 Parameters for active control of fundamental breakdown

$\epsilon\Theta_0$	$\epsilon\Theta_1$	$\Delta\phi_0$, rad	$\Delta\phi_1$, rad
30/31	0	3.5563	——
0	10/11	——	6.1781

dimensional control input. For both cases only in-phase control is considered. Table 3 summarizes the control parameters for the two cases. The first row represents the two-dimensional control case, and the second row represents the three-dimensional control case. For the two-dimensional case, the two-dimensional amplitude input ϵ_{θ_0} represents a temperature input of 30°C heating above the freestream with a steady-state heating of 31°C. The heater strip covers about one-half of the two-dimensional streamwise wavelength. For the three-dimensional control case, the three-dimensional amplitude input ϵ_{θ_1} represents a 10°C heating above the freestream temperature, with a steady-state overheat of 11°C. The three-dimensional heater strip covers one-half of the three-dimensional streamwise wavelength. The length of the heater strip is chosen based on the receptivity study. Several tests were made to determine an appropriate heating level. The level of heating is high, but the heater strip is not in a region of strong amplification, or a lower heat input would have been sufficient. The three-dimensional amplitude level that is generated from the heater strip closely matches the amplitude level of the uncontrolled three-dimensional flow for fundamental breakdown. The two-dimensional heat input is not sufficient to create the nonlinear amplitude level existing in the flow. The amplitude generated from the two-dimensional heater strip is about one-half as large as the uncontrolled amplitude level. Also, it was found in test calculations that increased heat input to the heater strip did not result in the same increase in disturbance amplitude levels. At higher temperatures, the viscosity variation with temperature is not as strong and the higher levels of heating become less effective. However, additional heater strips could be used to reduce the two-dimensional levels further.

The phase adjustment is different in form when compared with the small-amplitude active control investigations. For these nonlinear simulations a transfer parameter is used that is based on a method to determine transfer functions that Dittrich and Fasel[34] have successfully applied for active control of two-dimensional wave packet disturbances. Although the same method described for control of small-amplitude disturbances could be applied here, the phase is undergoing rapid changes downstream due to the nonlinear interactions, making the previous method less reliable. A downstream sensor again monitors the spanwise wall vorticity (or wall shear stress). The sensor is located approximately one wavelength downstream of the actuator. The transfer parameter is for a single-frequency wave and is implemented in the following manner. First, a numerical simulation run is made with the heater strip only. The transfer parameter is determined from the disturbance flow as follows:

$$\hat{H} = \frac{\hat{\Omega}^1_{z_k}(x_S, y=0)}{\hat{T}^1_k(x_{HS_C}, y=0)} \tag{22}$$

where $\hat{\Omega}^1_{z_k}(x_S, y=0)$ is the complex amplitude of the spanwise wall vorticity at the location of the sensor, and $\hat{T}^1_k(x_{HS_C}, y=0)$ is the complex amplitude of the wall temperature at the center of the heater strip. This transfer parameter is linear and represents the downstream response of the spanwise wall vorticity to the local temperature perturbations. To determine the appropriate phase adjustments that should be made for active control, the spanwise vorticity at the sensor is monitored with the disturbances emanating from the suction and blowing strip. The complex amplitude for this quantity $\hat{\Omega}^0_{z_k}(x_S, y=0)$ is then used to formulate the correct temperature input to the heater strip:

$$\hat{T}^2_k(x_{HS_C}, y=0) = -\frac{\hat{\Omega}^0_{z_k}(x_S, y=0)}{\hat{H}} \tag{23}$$

The minus sign denotes a 180-deg phase adjustment necessary for cancellation and is analogous to choosing $j=1$ for the

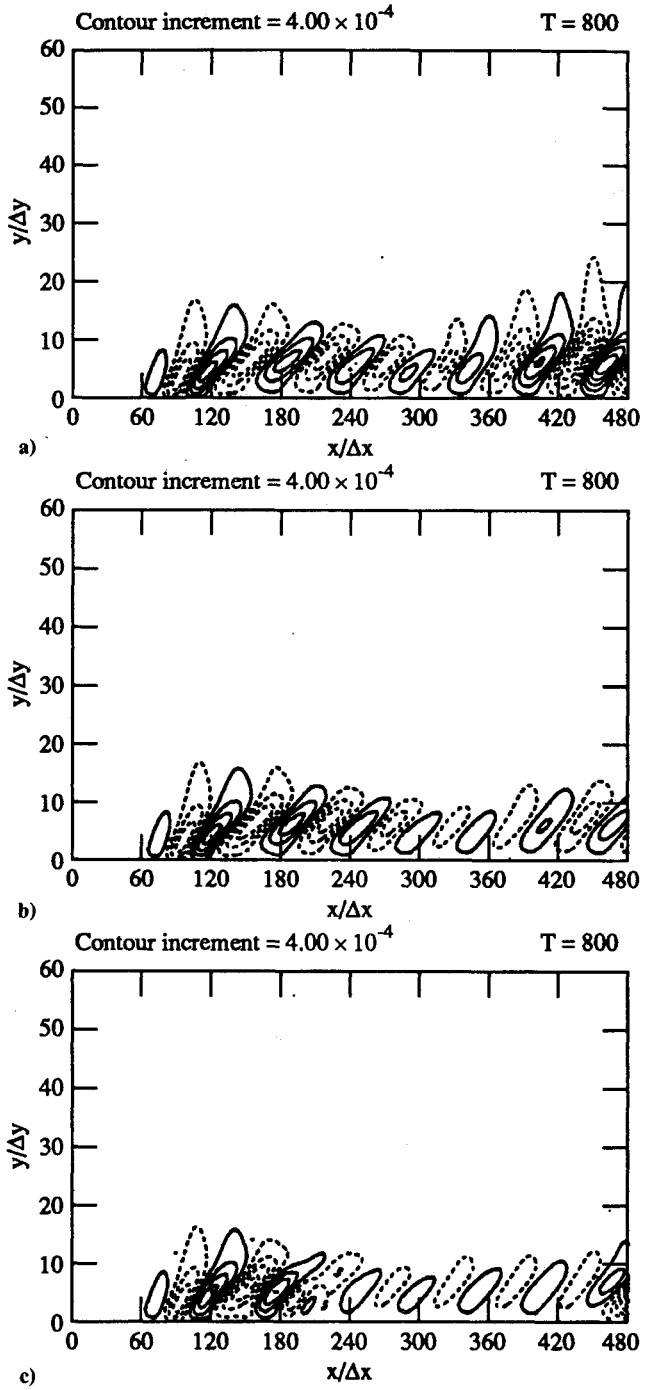

Fig. 9 Comparison of spanwise velocity w at $z = \lambda_z/4$ for fundamental breakdown: a) without control applied; b) with two-dimensional active control applied; and c) with three-dimensional active control applied.

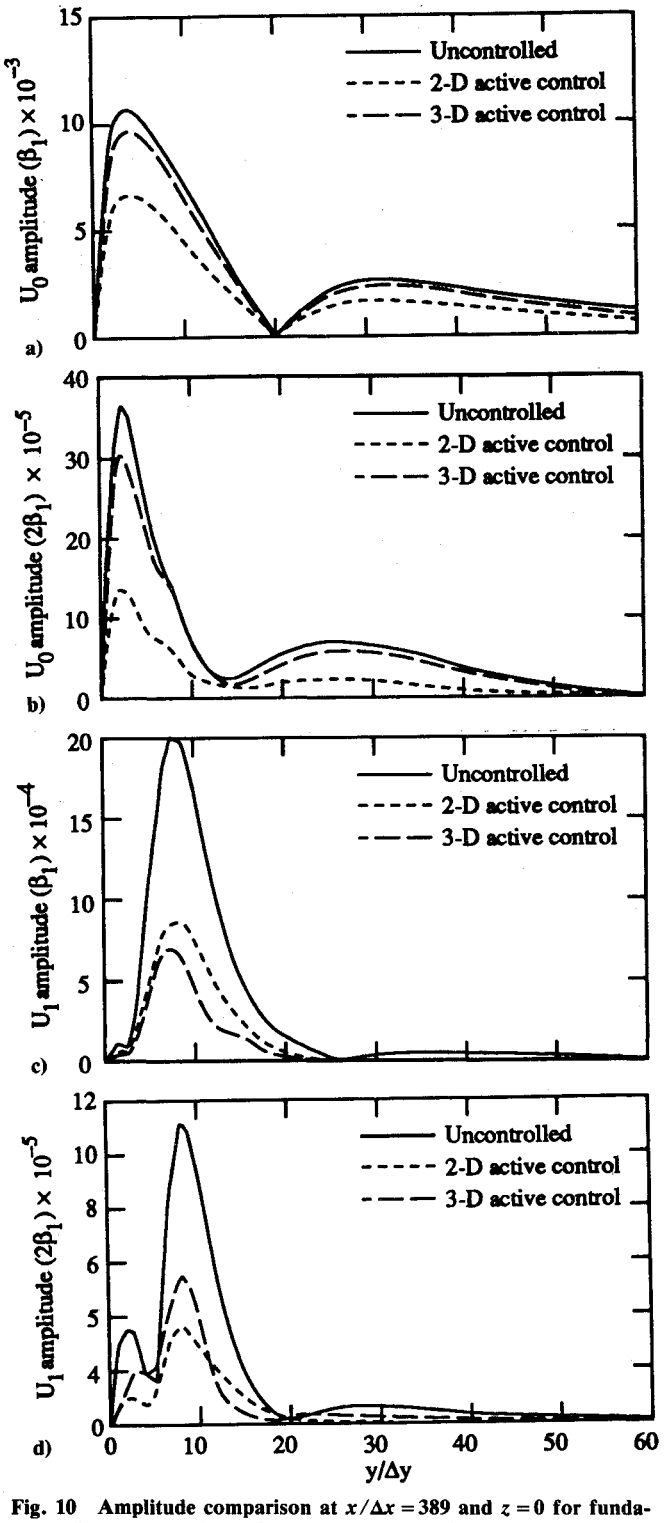

Fig. 10 Amplitude comparison at $x/\Delta x = 389$ and $z = 0$ for fundamental breakdown with active control applied: a) for two-dimensional velocity U_0 and β_1; b) for two-dimensional velocity U_0 and $2\beta_1$; c) for three-dimensional velocity U_1 and β_1; and d) for three-dimensional velocity U_1 and $2\beta_1$.

small-amplitude case. From this complex temperature, amplitude and phase adjustments to the heater strip can then be determined. However, the amplitude levels are not adjusted in the active control simulations because unreasonably high temperature inputs would be required for the two-dimensional active control case. The phases shown in Table 3 are determined from Eq. (23). The phase is calculated from

$$\Delta\phi_k = \tan^{-1}\left[\frac{\mathrm{Im}(\hat{T}_k^2)}{\mathrm{Re}\,(\hat{T}_k^2)}\right] \tag{24}$$

The procedure for determining the transfer parameter is carried out for both the two-dimensional and three-dimensional heater strips. Results of both simulations are now shown.

First, contours of the spanwise w velocity at the peak plane in the spanwise direction are shown in Fig. 9. The uncontrolled flow is shown in Fig. 9a, and the two-dimensional and three-dimensional active control cases are shown in Figs. 9b and 9c, respectively. Comparison of these three cases shows that a significant reduction in amplitude level and growth rates for both active control cases has occurred.

To more closely examine the effect of active control on the fundamental breakdown process, amplitude profiles for the U_k velocity are shown in Fig. 10 for both active control cases, as well as for the uncontrolled case. Comparison is made at $x/\Delta x = 389$. Both the amplitude at the fundamental frequency $\beta_1 = 0.588$ and the first harmonic $\beta_2 = 2\beta_1$ are shown for both the two-dimensional and three-dimensional wave components. The amplitude levels of the U_0 velocity are reduced with either two-dimensional or 3-dimensional control applied. Although only an oblique temperature perturbation has been introduced at the heater strip for the three-dimensional active control case, a two-dimensional steady-state component is also present. This steady-state component remained very local to the heater strip in the small-amplitude active control investigations due to the lower heating levels required. The steady-state overheat in the nonlinear investigations is larger and convects farther downstream. An analysis of the mean u velocity has revealed fuller velocity profiles over the heater strip and downstream of the heater strip. A linear stability analysis of the mean flow has verified that the heated profile is providing a stabilizing influence. Therefore, the two-dimensional amplitude is also slightly controlled with three-dimensional active control applied. This passive control effect provides an additional enhancement in stability because the two-dimensional amplitude levels control the three-dimensional growth rates. Also, it is noted that the two-dimensional periodic heating has caused a significant reduction in amplitude levels of both the fundamental frequency and the first harmonic. The important aspect to consider is the influence of active control on the three-dimensional components. Considering Figs. 10c and 10d, the three-dimensional amplitude levels for both the fundamental frequency and the first harmonic are significantly reduced with active control applied. The three-dimensional control input shows a slightly stronger reduction than two-dimensional control. For the two-dimensional control case, the three-dimensional disturbance is reduced by lowering the two-dimensional amplitude below the threshold limit where three-dimensional resonance growth can occur. In the three-dimensional control case, the three dimensional disturbance is directly attenuated due to the antiphased oblique temperature perturbations introduced at the actuator. However, to fully compare the two control simulations, the effect on the flowfield even further downstream must be considered.

Conclusions

A numerical method has been developed ot study the influence of control in the spatially evolving boundary layer. Active methods of control using surface heating techniques have been numerically investigated. Numerical simulations of active control of small-amplitude two-dimensional T-S waves and three-dimensional oblique waves have shown that periodic surface heating can be an effective method of transition control. Localized periodic wall temperature perturbations antiphased with the disturbances present in the flow resulted in a significant reduction in the amplitude levels in the flow. A receptivity study of a surface heater strip shows that the boundary layer is more receptive to smaller heater strips in that the narrower strips maximized the disturbance levels generated in the flowfield. Numerical simulations of active control of the fundamental breakdown process showed active control using periodic surface heating to be a viable technique for control at the early stages of nonlinear secondary instabil-

ity. Either two-dimensional or three-dimensional localized temperature perturbations were used, with the three-dimensional control input providing a slightly more stabilizing influence than the two-dimensional control input. Because of the high level of heating required to bring down the two-dimensional amplitudes, two-dimensional active control is less efficient than three-dimensional active control in terms of power input required.

Acknowledgments

This research was sponsored by the NASA Graduate Student Researchers Program (NASA Grant NGT-03002809) and the Office of Naval Research (ONR Grant N00014-K-0515). The computer resources for this work were provided by the NASA Ames Research Center. This support is gratefully acknowledged.

References

[1]Wehrmann, O. H., "Tollmien-Schlichting Waves Under the Influence of a Flexible Wall," *Physics of Fluids*, Vol. 8, 1965, pp. 1389–1390.

[2]Schliz, W., "Experimentelle Untersuchungen zur Akustischen Beeinflussung de Strömungsgrenzschicht in Luft," *Acustica*, Vol. 16, 1965/66,
pp. 208–223.

[3]Milling, R. W., "Tollmien-Schlichting Wave Cancellation," *Physics of Fluids*, Vol. 24, No. 5, 1981, pp. 979–981.

[4]Gedney, C. J., "The Cancellation of a Sound-Excited Tollmien-Schlichting Wave with Plate Vibration," *Physics of Fluids*, Vol. 26, No. 5, 1983, pp. 1158–1160.

[5]Strykowski, P. J., and Sreenivasan, K. R., "The Control of Transitional Flows," AIAA Paper 85-0559, March 1985.

[6]Maestrello, L., "Active Transition Fixing and Control of the Boundary Layer in Air," AIAA Paper 85-0564, March 1985.

[7]Liepmann, H. W., Brown, G. L., and Nosenchuck, D. M., "Control of Laminar-Instability Waves Using a New Technique," *Journal of Fluid Mechanics*, Vol. 118, 1982, pp. 187–200.

[8]Thomas, A. S. W., "The Control of Boundary-Layer Transition Using a Wave-Superposition Principle," *Journal of Fluid Mechanics*, Vol. 137, 1983, pp. 233–250.

[9]Liepmann, H. W., and Nosenchuck, D. M., "Active Control of Laminar-Turbulent Transition," *Journal of Fluid Mechanics*, Vol. 118, 1982, pp. 201–204.

[10]McMurray, J. T., Metcalfe, R. W., and Riley, J. J., "Direct Numerical Simulations of Active Stabilization of Boundary Layer Flows," *Proceedings of the Eighth Biennial Symposium on Turbulence*, Univ. of Missouri at Rolla, Rolla, MO, 1983.

[11]Bayliss, A., Maestrello, L., Parikh, P., and Turkel, E., "Numerical Simulation of Boundary Layer Excitation by Surface Heating/Cooling," AIAA Paper 85-0565, March 1985.

[12]Bower, W. W., Kegelman, J. T., Pal, A., and Meyer, G. H., "A Numerical Study of Two-Dimensional Instability-Wave Control Based on the Orr-Sommerfeld Equation," *Physics of Fluids*, Vol. 30, No. 4, 1987, pp. 998–1004.

[13]Bower, W. W., Pal, A., Cain, A. B., and Meyer, G. H., "Two-Dimensional Multifrequency Instability Suppression Via Surface Mass Transfer: Linear Theory and Its Application," *Mathematial Computational Modelling*, Vol. 11, 1988, pp. 170–174.

[14]Pal, A., Bower, W. W., Cain, A. B., and Meyer, G. H., "Numerical Simulations of Instability-Wave Suppression in the Blasius Boundary Layer," *Proceedings of the Eleventh Symposium on Turbulence*, Univ. of Missouri at Rolla, Rolla, MO, 1988.

[15]Bower, W. W., Pal, A., and Meyer, G. H., "Computations of Two-Dimensional Instability-Wave Control Through Surface Heating," *Proceedings of the Twentieth Midwestern Mechanics Conference*, Purdue Univ., West Lafayette, IN, 1987.

[16]Kleiser, L., and Laurien E., "Three-Dimensional Numerical Simulation of Laminar-Turbulent Transition and its Control by Periodic Disturbances," *Proceedings of the Second IUTAM Symposium on Laminar-Turbulent Transition*, Springer-Verlag, Berlin, 1984.

[17]Kleiser, L., and Laurien, E., "Numerical Investigation of Interactive Transition Control," AIAA Paper 85-0566, March 1985.

[18]Biringen, S., Nutt, W. E., and Caruso, M. J., "Transition Control by Periodic Suction-Blowing," AIAA Paper 85-1700, July 1985.

[19]Zang, T. A., and Hussanini, M. Y., "Numerical Experiments on Subcritical Transition Mechanism," AIAA Paper 85-0296, Jan. 1985.

[20]Zang, T. A., and Hussaini, M. Y., "Numerical Experiments on the Stability of Controlled Shear Flows," AIAA Paper 85-1698, July 1985.

[21]Fasel, H., Rist, U., and Konzelmann, U., "Numerical Investigation of the Three-Dimensional Development in Boundary Layer Transition," *AIAA Journal*, Vol. 28, No. 1, 1990, pp. 29–37.

[22]Robey, H. F. III, "On the Nature of Oblique Instability Waves in Boundary Layer Transition," Ph.D. Dissertation, Graduate Aeronautical Lab., California Inst. of Technology, Pasadena, CA, 1986.

[23]Corke, T. C., "Resonant Three-Dimensional Modes in Transitioning Boundary Layers—Structure and Control," AIAA Paper 89-1001, March 1989.

[24]Morkovin, M. V., "Critical Evaluation of Transition from Laminar to Turbulent Shear Layers with Emphasis on Hypersonically Travelling Bodies," Air Force Flight Dynamics Lab. Rept. AFFDL-TR-68-149, Wright-Patterson AFB, OH, 1969.

[25]Heinrich, R. A., Choudari, M., and Kerschen, E. J., "A Comparison of Boundary Layer Receptivity Mechanisms," AIAA Paper 88-3758, July 1988.

[26]Wlezien, R. W., "Measurement of Boundary-Layer Receptivity at Suction Surfaces," AIAA Paper 89-1006, March 1989.

[27]Klebanoff, P. S., Tidstrom, K. D., and Sargent, L. M., "The Three-Dimensional Nature of Boundary-Layer Instability," *Journal of Fluid Mechanics*, Vol. 12, No. 1, 1962, pp.1–41.

[28]Hardy, R. C., and Cottington, R. C., "Viscocity of Deuterium Oxide and Water in the Range 5° to 125° C," *Journal of Research of the National Bureau of Standards,* Vol. 42, June 1949, pp. 573–578.

[29]Swindells, J. F., National Bureau of Standards, private communication.

[30]Kral, L. D., "Numerical Investigation of Transition Control of a Flat Plate Boundary Layer," Ph.D. Dissertation, Dept. of Mechanical and Aerospace Engineering, Univ. of Arizona, Tucson, AZ, 1988.

[31]Chouradi, M., and Kerschen, E. J., "Instability Wave Patterns Generated by Interaction of Sound Waves with Three-Dimensional Wall Suction or Roughness," AIAA Paper 90-0119, Jan. 1990.

[32]Nosenchuck, D. M., "Passive and Active Control of Boundary Layer Transition," Ph.D. Dissertation, Graduate Aeroanutical Lab., California Inst. of Technology, Pasadena, CA, 1982.

[33]Maestrello, L., "Analysis of Active Control by Surface Heating," AIAA Paper 84-0173, Jan. 1984.

[34]Dittrich, P. A., and Fasel, H. F., "Numerical Simulation of Wave Packet Control in a Flat Plate Boundary Layer," *Bulletin of the American Physical Society,* Vol. 33, No. 10, 1988.